Geometric Calibration of a Structured Light System Using Circular Control Points

Jean-Nicolas Ouellet Félix Rochette Patrick Hébert
Computer Vision and Systems Laboratory, Laval University, Québec, Canada
{jouellet,hebert}@gel.ulaval.ca, felix.rochette.1@ulaval.ca

Abstract

We present a new geometric calibration method for a structured light system combining a projector with a camera, using a planar target with circular control points. By solely exploiting the mapping between projected conics, the proposed method is strictly geometric and provides unbiased camera to projector correspondences during its application. Such a geometric method does not rely on radiometric calibration. Moreover, the method consistently ensures uniform coverage of the working volume and automatically avoids interference between both the projected and the printed patterns on the calibration target.

1. Introduction

Since they can provide full field 3D range images, structured light systems (SLS) are frequently used for capturing the 3D shape of static or moving objects [4, 14, 9, 11, 13]. SLS are typically composed of a controllable white light projector and one or more cameras. When only one camera is used along with the projector, the ensemble must be geometrically calibrated to provide accurate 3D measurements from triangulation. Several calibration methods have been published for that purpose [12, 10, 5]. They mainly differ in the type of target and procedure, the projected pattern, and the projector model.

We propose a rigorous method that is easy to apply and that makes it possible to calibrate using a planar target with circular control points. For their higher accuracy, circular control points are of common use in camera calibration for photogrammetric applications [3]. In this context, one must be aware that the projection of the center of a circle does not correspond to the center of the ellipse in the image. This subpixel bias is systematic and depends on the viewpoint, the optics of the system and the size of the control point. In order to eliminate such a bias, Heikkila proposed in [3] to model the projection of the conic contour rather than its center during the calibration. In this paper, we extend the method to calibrate a camera-projector pair.

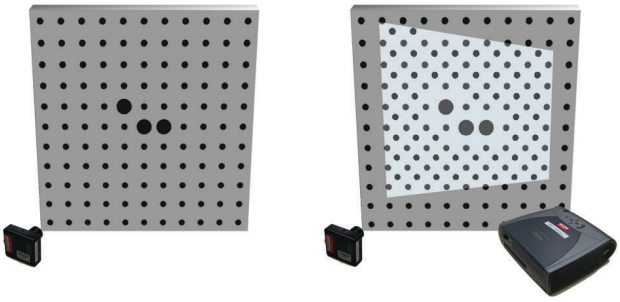

(a) (b)

Figure 1. (a) The camera is calibrated from a planar target printed with a pattern of circular control points. (b) The projection of an adapted pattern of ellipses instantiates a second set of circular points on the target without interfering with the printed pattern.

Although the projector can be calibrated as a second camera, all observations must be collected by the camera and thereby, one must determine the correspondence between pixels in the camera and projector. Some methods have been proposed for calibrating SLS with circular control points [5, 2]. None of these methods exploits the homography between the ellipses' contours in the camera and projector. Actually the correspondence is usually obtained by applying a phase-shift technique to match the center of the ellipse with its corresponding point in the projector. It must then be assumed that this point corresponds to the center of the circle on the calibration target. Besides introducing the biased center, the phase-shift approach relies on radiometric calibration for subpixel accuracy.

Alternatively, we propose to use the same target with black circular points on a light background that is typically used in camera calibration. From the projector, cir-

cular points are projected between the printed black points and then observed by the camera (see Fig.1(b)). It is therefore possible to exploit the camera-to-projector homography to map the conic between the two devices, thus avoiding the biased center. Moreover, we avoid the explicit calculation of 3D points on the target. Since it is then possible to calibrate the projector as a second camera, the calibration target is displaced in the working volume and the system is calibrated as a stereo pair. The intrinsic parameters and the projector-to-camera transformation are finally optimized using bundle adjustment.

During the calibration procedure, one must avoid the overlap between projected and printed points on the target. Such overlap causes interference between the two patterns and affects the accuracy of the detected ellipses in the image. For this reason, the system automatically adapts the projected control points to interleave between black circles on the target. Besides avoiding interference, both printed and projected circular points are distributed uniformly on the target and thus within the working volume. Moreover, rather than projecting circles, the calibration system further adapts by projecting ellipses that will map to circles on the calibration target (see Fig.1). By doing so, we avoid high eccentricity ellipses in the observed image when the target is rotated.

Since it is automated, the procedure is very simple to apply and only requires a planar target with dark circular control points. In the sequel, a review of existing approaches is presented along with their limitations. The details of the proposed approach and its implementation follow in section 3 before the results section.

2. Related work

A usual method to reconstruct an object with structured light consists in projecting multiple stripes on the object. Triangulation is then performed between the ray cast from the edge points of the deformed stripe in the camera image and its corresponding plane cast from the projector image. In [12], it is proposed to model each projected stripe individually with four parameters describing the stripe plane in the camera reference frame. To accomplish this, the camera is first calibrated from the printed pattern of a 3D target. The target consists of two perpendicular planes and it is oriented such that the projection of a stripe illuminates both planes. The points of an imaged stripe are back-projected from the camera to the target and its corresponding plane parameters are estimated from the 3D points. Although intuitive, this model quickly becomes inadequate and over parameterized when each column or line of the projector image are to be modeled.

Instead of modeling each stripe individually, in [11, 4] it is proposed to estimate a global 2x4 transformation matrix describing the relationship between the 3D world points and the 1D stripe coordinates of the projector. This model is a 1D camera pinhole and it gathers all of the planes in a single representation. To recover the 1D pinhole parameters, the camera is first calibrated from a 3D target. The target consists of two perpendicular planes printed with a checkerboard pattern. Then, stripes are projected on the target and their corresponding 3D points are obtained by back-projection from the camera image. The 1D to 3D correspondences provide enough constraints to calibrate the 1D pinhole. It is interesting to notice that in [4], interfering stripe points that were projected over the printed pattern are not considered for the calibration. Still, the accuracy of the calibration method relies on the accuracy of the stripe localization in the camera image.

In [10], a checkerboard pattern is projected on the target instead of stripes. The localization of such calibration markers is more accurate than the edges of a stripe. The projector is calibrated as a 2D pinhole. The target consists in a plane where the first half is printed with the calibration pattern and the second half is white. This white section of the target is placed in front of the projector while the pattern is projected. The pose of the pre-calibrated camera is computed from the printed pattern, which allows the projected pattern to be back-projected from the camera to the target. This process is repeated for three or more views of the target, gathering enough 2D-3D correspondences to recover the projector parameters with a standard camera calibration method [15]. This method exhibits an important issue; the projected markers should be localized accurately and free from interference with the printed pattern. However, the recovered parameters are optimized only in the calibration volume of the projector, which is different from the combined working volume with the camera. A small error in the camera pose will result in a larger error in the recovered 3D marker coordinates. This motivates the projection of an adapted calibration pattern directly in the printed region of the target while covering the working volume.

The methods proposed in [2, 5] attempt to eliminate the latter problem by exploiting the same markers to calibrate both the camera and projector. They use white circular control points printed on a dark planar target. After projecting light on the target, ellipses corresponding to the circular points are extracted in the camera image. Then, a phase-shift technique is applied to match the center of the ellipse with its corresponding point in the projector. The centers of the detected ellipses are assumed to correspond to the 3D center of the target circles. This allows the projector to be calibrated as a 2D pinhole from the correspondences between the 3D markers and the projector coordinates obtained from the phase-shift. However, due to projective deformation, the detected ellipse centers in the camera image do not correspond to the 3D circle centers. The phase-shift

algorithm wrongly associates the 3D marker centers thus introducing a bias. The bias can be eliminated in the case of camera calibration by projecting the conic equation of the circular contour instead of the marker center [3]. Still, the phase-shift algorithm cannot yield the corresponding ellipse center coordinates in the projector image since it is not directly observable in the camera image. To solve this problem, one could use a printed checkerboard pattern which is not affected by the bias, but phase-shift methods are inaccurate near edges and dark regions.

An acceptable alternative is to project a checkerboard interleaved within the same printed pattern and observe it with the camera. A homography could then be exploited to map the observed pattern between the camera and the projector. In this context, the projection of circles instead of a checkerboard pattern will lead to better accuracy. Actually, for an image region of the same size, the localization of a circle benefit from a longer contour when compared to the edges of the checkerboard. Moreover, sensitivity to position and orientation due to image discretization is reduced. In a simulation where images of both patterns were generated at random positions and orientations, we observed that ellipse centers were on average ten times more accurate. In the next sections it is shown how to calibrate a SLS using circular points without introducing a bias.

3. SLS calibration

In this section, we first describe the projection model of the camera and projector, before explaining the procedure to recover their parameters. The superscript 'c' and 'p' will be added to discriminate between the parameters of the camera and projector respectively. By the same token, the subscripts 'c', 'p' and 'w' (world-target) will be used to specify the reference frame when necessary.

3.1. Camera model

The projection model of the camera is a pinhole with lens distortion compensation. The pinhole model describes the relationship between a 3D point $\widetilde{\mathbf{P}}_w = [X, Y, Z, 1]^T$ in the world reference frame and the corresponding image point $\widetilde{\mathbf{a}} = [u, v, 1]^T$. Here, the tilde superscript indicates homogeneous coordinates. The relation is a projection defined as $\lambda\widetilde{\mathbf{a}} = \mathbf{K}\left[\begin{array}{cc}\mathbf{R} & \mathbf{t}\end{array}\right]\widetilde{\mathbf{P}}$. In this equation, the matrix $\mathbf{K} = \begin{bmatrix}\alpha & 0 & u_0\\ 0 & \beta & v_0\\ 0 & 0 & 1\end{bmatrix}$ includes the camera intrinsic parameters, where (u_0, v_0) are the coordinates of the principal point, α and β are the scale factors of the image horizontal and vertical axes, $(\mathbf{R}, \mathbf{t})$ are the 3x3 rotation matrix and 3x1 translation vector describing the transformation from the world to the camera reference frame, and λ is an arbitrary scale factor. To calibrate the model, we use a planar target assumed to lie on the plane $Z = 0$. Thus, the 3x4 projection matrix reduces to a 3x3 homography. If we denote the ith column of the rotation matrix $\mathbf{R}$ by $\mathbf{r}_i$, the reduced transformation is given by [15]:

$$\mathbf{K}\left[\mathbf{r}_1 \;\; \mathbf{r}_2 \;\; \mathbf{r}_3 \;\; \mathbf{t}\right]\begin{bmatrix}X\\Y\\0\\1\end{bmatrix} = \mathbf{K}\left[\mathbf{r}_1 \;\; \mathbf{r}_2 \;\; \mathbf{t}\right]\begin{bmatrix}X\\Y\\1\end{bmatrix}, \quad (1)$$

with the homography $\mathbf{H} = \mathbf{K}\left[\mathbf{r}_1 \;\; \mathbf{r}_2 \;\; \mathbf{t}\right]$. In practice, due to lens distortion, a point is not imaged at coordinates $\mathbf{a}$ predicted by the projection, but at distorted coordinates $\mathbf{a}_d$. To compensate for the distortion, the projection model is augmented with two radial (k_1, k_2) and two tangential terms (p_1, p_2). These four additional intrinsic parameters are represented in a vector $\mathbf{d}$. The coordinates $\mathbf{a}_d$ can then be corrected using the following relation $\mathbf{a} = \mathbf{a}_d - \delta(\mathbf{a}_d, \mathbf{d})$ where

$$\delta(\mathbf{a}_d, \mathbf{d}) = \begin{bmatrix} x_d(k_1 r_d^2 + k_2 r_d^4) + 2p_1 x_d y_d + p_2(r_d^2 + 2x_d^2) \\ y_d(k_1 r_d^2 + k_2 r_d^4) + 2p_2 x_d y_d + p_1(r_d^2 + 2y_d^2) \end{bmatrix}, \quad (2)$$

and $[x_d, y_d, 1]^T = \mathbf{K}^{-1}[u_d, v_d, 1]^T$ and $r_d^2 = x_d^2 + y_d^2$. Computing the distortion in normalized coordinates improves the conditioning of the system when solving for the parameters of the model. During the calibration process, distortion must also be added to points, but there are no direct methods to inverse the distortion function. In [3], an inverse model based on a Taylor series approximation is proposed. However, for short focal lens with significant distortion, the method complexifies due to the need of additional terms in the series development. An alternative method, simple and very accurate, is to recursively approximate the inverse solution. The additional calculation is not problematic in the context of offline calibration. The recursion equations are:

$$\mathbf{a}_d \approx \mathbf{a} + \delta(\mathbf{a}_d, \mathbf{d}) \approx \mathbf{a} + \delta(\mathbf{a} + \delta(\mathbf{a}_d, \mathbf{d}), \mathbf{d}) \approx \cdots . \quad (3)$$

In our implementation, we use 10 iterations to generate the inverse mapping.

To lighten the notation in the next sections, we group the camera intrinsic parameters in a single vector $\theta^c = \{\alpha, \beta, u_0, v_0, k_1, k_2, p_1, p_2\}$, and the extrinsic parameters in $\Theta^c = \{\mathbf{r}_{xyz}, \mathbf{t}\}$. Here, $\mathbf{r}_{xyz}$ is a three element vector of a minimal representation for the rotation $\mathbf{R}$. We have chosen to use the canonical exponential coordinates given by Rodrigues' formula [6]; quaternions are also adequate.

During the calibration process, the camera model will be used to project ellipses $\mathbf{E}_w$ from the target to the camera image as well as to add distortion to the coordinates of the resulting ellipses' centers to obtain the distorted point $\mathbf{a}_d$. For this purpose, we introduce the function G_c such that

$\mathbf{a}_d = G_c(\mathbf{E}_w, \theta, \Theta)$. In the function, an ellipse is projected using a homography constructed from the reduced projective transformation in Eq.1. A homography $\mathbf{H}$ transforms a 3x3 ellipse $\mathbf{E}$ to $\mathbf{E}'$ as follows:

$$\mathbf{E}' = \mathbf{H}^{-T}\mathbf{E}\mathbf{H}^{-1}. \quad (4)$$

After the projection, the distortion is added to the ellipse center. The center is extracted by the multiplication of the ellipse inverse $\mathbf{E}^{-1}$ with the vector $[0\ \ 0\ \ 1]^T$ [3]. For convenience, we include the following expression of the 3x3 conic matrix of a circular marker $\mathbf{E}$ of radius r centered at coordinates (x, y) since it will be required in the procedure:

$$\mathbf{E} = \begin{bmatrix} \frac{-1}{r^2} & 0 & \frac{x}{r^2} \\ 0 & \frac{-1}{r^2} & \frac{y}{r^2} \\ \frac{x}{r^2} & \frac{y}{r^2} & \frac{r^2-(x^2+y^2)}{r^2} \end{bmatrix}. \quad (5)$$

3.2. Projector model

The projector is modeled as an inverse pinhole camera with lens distortion. Therefore, the model developed in the previous section applies and one obtains the projector intrinsic parameters $\theta^p = \{\alpha^p, \beta^p, u_0^p, v_0^p, k_1^p, k_2^p, p_1^p, p_2^p\}$ and extrinsic parameters $\Theta^P = \{\mathbf{r}^p_{xyz(c)}, \mathbf{t}^p_c\}$. The extrinsic parameters describe the pose of the projector in the camera reference frame.

In order to obtain the projector model parameters, observed ellipses are projected from the camera image to the projector image. The relation between both images is a homography induced by the target plane. This homography involves the intrinsic and extrinsic parameters of both, the camera and the projector, as well as the plane orientation with respect to the camera. It is recovered from the following relation [6]:

$$\mathbf{H}_{cp} = \mathbf{K}^p \left[\mathbf{R}^p_c - \mathbf{t}^p_c \frac{1}{d}\mathbf{N}^T\right] (\mathbf{K}^c)^{-1}, \quad (6)$$

where $(\mathbf{N}, d)$ are the target plane parameters expressed in the camera reference frame. The parameters of the plane are obtained from the camera pose with respect to the target reference frame $(\mathbf{R}^c_w, \mathbf{t}^c_w)$. The plane normal vector is given by $\mathbf{N} = [r^c_{13}, r^c_{23}, r^c_{33}]^T$ and its distance to origin by $d = -[r^c_{31}\ \ r^c_{32}\ \ r^c_{33}]\mathbf{t}^c_w$. Under this notation, a 3D point $\mathbf{P}$ on the plane verifies $\mathbf{N}^T\mathbf{P} + d = 0$.

During the calibration process, the projector model will be exploited to project ellipses from the distorted camera image to the undistorted projector image. More precisely, the ellipses observed in the camera image are first undistorted with the camera parameters[1], then transferred to the projector with the homography from Eq.6. Finally, the resulting ellipses are undistorted with the projector parameters and their center is extracted to obtain the points $\mathbf{a}^p$. We summarize these steps with the function G^p such that $\mathbf{a}^p = G^p(\mathbf{E}_c, \theta^c, \Theta^c, \theta^p, \Theta^p)$.

[1] Two approaches to remove distortion from an ellipse are discussed in section 4.

3.3. Calibration target

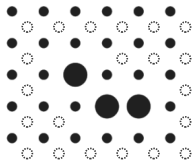

Figure 2. Pattern of the calibration target. The virtual control points, shown as dotted circles, are not visible on the actual target and will be instantiated by the projector.

The calibration target consists in a white diffuse plane printed with dark circular markers, as displayed in Fig.1(a). The size of the printed markers is chosen such that their diameters typically vary between 20-40 pixels in the image. The notable characteristic of the target is the presence of virtual circular control points, depicted as dotted circles in Fig.2. These markers are part of the target model to simplify the generation of the pattern to project; they are not visible on the actual target. As it is displayed in Fig.1(b)), they will be instantiated by the projector during the calibration procedure. In the pattern, the three large circles define an affine basis that is easy to recognize from any view of the target. The control points are then progressively matched from these three ellipses toward the border of the image.

3.4. Calibration procedure

3.4.1 Data acquisition

The calibration of the SLS requires observations from three or more views of the planar target. For each image, we need to extract the two series of ellipses corresponding to the printed and virtual markers. The ellipses corresponding to the printed markers are easily extracted under the projection of uniform white light (see Fig.3). However, to make the virtual markers visible to the camera, we need to synthesize an image of the virtual markers as they would be seen by the projector and then reproject them. This is possible is we recover the approximate homography between the target and projector. In this context, an approximation of the homography is sufficient since we aim mainly to avoid interference of the projected pattern with the printed markers.

The three steps that are necessary to recover the target-to-projector homography are now described.

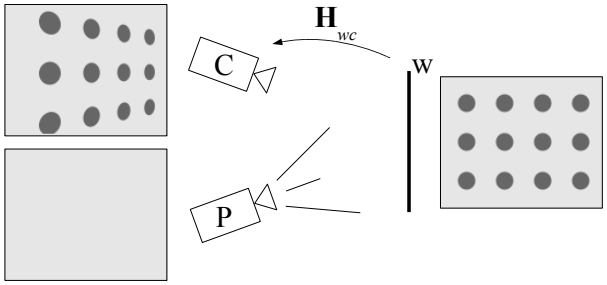

Figure 3. Data acquisition (1/3): a) A white image is projected on the target to recover a first estimate of the homography $\mathbf{H}_{wc}$. The camera and projector images are in the top and bottom left respectively, and a view of the calibration target is on the right. The printed pattern is depicted in gray.

The first step consists in recovering the target-to-camera homography $\mathbf{H}_{wc}$. This homography is directly estimated from the centers of the printed markers on the target $\mathbf{a}_w^c$ and their corresponding centers in the camera image $\mathbf{a}_c^c$. At this point, it is not necessary to consider the projection asymmetry of ellipses. However, to compensate for the radial distortion of the camera, we also estimate a single radial distortion term k_1^c expressed with respect to the image center. The homography and distortion term are obtained with a standard non-linear optimization [15].

Once the homography $\mathbf{H}_{wc}$ is obtained, the second step consists in approximating the camera-to-projector homography $\mathbf{H}_{cp}$. This is done by projecting a regular grid of black disks on the target as shown in Fig.4. The projected markers are identified in the camera image by background subtraction from the initial image. The centroid points of the identified regions are extracted and undistorted with k_1^c. A coarse estimate of the camera-to-projector homography $\mathbf{H}_{cp}$ is then computed from the correspondence between the undistorted centroid points in the camera image and the circle centers in the projector image. At this point, the segmentation needs not to be perfect for all ellipses. The recovered homography only aims to project circles between the printed pattern and will be discarded afterwards.

In the third step, the target-to-projector homography $\mathbf{H}_{wp}$ is computed by combining the previous homographies as $\mathbf{H}_{wp} = \mathbf{H}_{cp}\mathbf{H}_{wc}$. This allows the virtual circular markers to be projected from the target to the projector image. An image of the desired ellipses is synthesized and reprojected on the target (see Fig.5). The camera then acquires an image of the target and the ellipses corresponding to the virtual markers are extracted and matched with the ellipse centers in the projector image. This final correspondence will be used for the precise calibration of the projector in a global optimization. Still, in order to initialize the optimization the projector needs to be precalibrated in the same reference frame as that of the camera. Thus, the ellipses corresponding to the virtual markers on the target are recovered by backprojecting the corresponding ellipses from the camera to the target with the homography $\mathbf{H}_{cw}$. After repeating these three steps for each view of the target, the acquisition is completed. Table 1 summarizes the information extracted for each view.

Table 1. Information extracted for each view of the target

		Description
Camera	$\mathbf{E}_w^c$	Printed markers on the target
	$\mathbf{a}_c^c$	Corresponding center coordinates in the camera image
Projector	$\mathbf{E}_c^p$	Virtual markers in the camera image
	$\mathbf{E}_w^p$	Corresponding ellipses on the target
	$\mathbf{a}_p^p$	Corresponding center coordinates in the projector image

3.4.2 Initialization

To initialize the parameter optimization, the camera and projector are calibrated separately with the method proposed in [3]. The camera is pre-calibrated from the correspondences between the printed ellipses of the target $\mathbf{E}_w^c$ and their centers in the camera image $\mathbf{a}_c^c$ whereas the projector is pre-calibrated from the correspondences between the virtual markers of the target $\mathbf{E}_w^p$ and their centers in the pro-

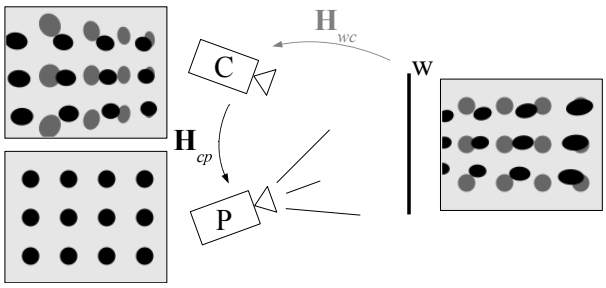

Figure 4. Data acquisition (2/3): A regular grid of circles is projected on the target to recover an approximation of the homography $\mathbf{H}_{cp}$. (See Fig.3 for more details)

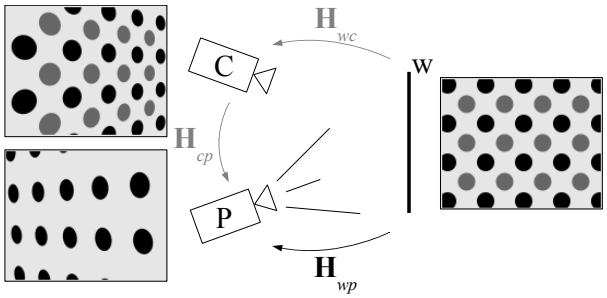

Figure 5. Data acquisition (3/3): The virtual markers are transferred from the target to the projector using the homography $\mathbf{H}_{wp}$ to synthesize an image of the virtual markers. The reprojection of the image instantiates the virtual markers. (See Fig.3 for image details)

jector image $\mathbf{a}_p^p$. Note that the initial principal point of the projector required by the routine in [3] should be shifted upward from the optical axis of the lens to reflect the position of the projector image with respect to the lens. The shift is usually available from the projector specifications. The initialization yields the intrinsic parameters of the camera and projector along with their poses relative to the target.

3.4.3 Optimization

The optimization finds the parameters of the SLS model $\varphi^{SLS} = \{\theta^c, \theta^p, \Theta^p, \Theta_1^c, \ldots, \Theta_M^c\}$ that minimize simultaneously the projection error in the camera and projector image for the O views of the target. The error to minimize is summarized by the following objective function:

$$J(\varphi^{SLS}) = \sum_k^O \left(\begin{array}{l} \sum_i^M \|\mathbf{a}_{c(ik)}^c - G^c(\mathbf{E}_{w(ik)}^c, \theta^c, \Theta_k^c)\|^2 + \\ \sum_j^N \|\mathbf{a}_{p(jk)}^p - G^p(\mathbf{E}_{c(jk)}^p, \theta^c, \Theta_k^c, \theta^p, \Theta^p)\|^2 \end{array} \right), \quad (7)$$

for M printed markers and N virtual markers in each image. The parameters minimizing Eq.7 are obtained by applying the Levenberg-Marquardt algorithm [8]. The pose of the projector relative to the camera Θ^p is computed from the initial parameters as

$$\begin{bmatrix} \mathbf{R}_c^p & \mathbf{t}_c^p \\ \mathbf{0} & 1 \end{bmatrix} = \begin{bmatrix} \mathbf{R}_w^p & \mathbf{t}_w^p \\ \mathbf{0} & 1 \end{bmatrix} \begin{bmatrix} \mathbf{R}_w^c & \mathbf{t}_w^c \\ \mathbf{0} & 1 \end{bmatrix}^{-1}.$$

We use the extrinsic parameters from the first view of the target. It is important to note that a single projector pose will be estimated for all calibration image pairs. This enforces the rigidity constraint of the system where the projector is rigidly fixed to the camera.

4. Results

To validate the calibration method, we first analyze the residual error after the optimization and the recovered distortion parameters. Then, a series of 3D reconstructions are performed to assess the overall accuracy of the system by comparing the reconstructed objects to precise 3D models measured with a 3D laser scanner.

The SLS used to generate the following results is composed of a PointGrey DragonFly2 greylevel camera mounted with a 12 millimeters (mm) lens and an InFocus LP350 projector. The resolution of both devices is 1024x768 pixels. The baseline of the SLS system is approximately 650mm and the devices are rotated so that their optical axes intersect at approximately 1500mm. The reconstructions were performed under the same ambient lighting that was present for the calibration. This is important to prevent any bias caused by chromatic aberration of the camera lens.

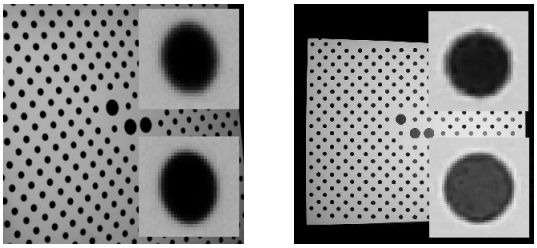

(a) (b)

Figure 6. The calibration target as seen by the camera from two viewpoints. The top-right and bottom-right insets are images of a virtual and printed marker respectively.

The calibration is performed from 21 images of the planar target acquired under different viewpoints. The number of images required for a repeatable calibration depends on the setup and should be evaluated once. To obtain this number, 50 calibration experiments were conducted from random subsets of images acquired from 42 different viewpoints. The calibration experiments were repeated using 5 to 30 images. The variance of the recovered parameters reached a minimum at 21 images. The ellipse parameters required by the calibration procedure are then estimated with the method presented in [7]. In Fig.6, it is possible to compare the virtual and printed markers as seen by the camera from two viewpoints. Although the virtual markers are slightly blurry, their shape and position make them almost impossible to distinguish from the actual printed markers.

When calibrating the system, there are two methods for processing ellipse distortion and both do not yield exactly the same ellipse positions. In the first method, a distortion

vector is computed for the current ellipse center and used to translate the ellipse. This is what is done in [3]. In the second method, the distortion is applied to the detected contour points before the ellipse is fitted. With our system and for an ellipse having a radius of 20 pixels located near the border of the camera image, the difference between both methods is in the order of 0.03 pixel. The small but systematic difference can be explained with the camera distortion curve in Fig.7 which shows the distortion magnitude with respect to the distance from the principal point. The magnitude for radii representing the two boundaries of an ellipse differs sufficiently to warp the ellipse along the radial direction and affects the fitting. We have implemented both methods but we did not observe significant improvement in the results. The precision of our target model is approximately equivalent to the difference. Nevertheless, the following results were generated with the second method.

The residual error vectors obtained after optimization had a mean and maximum magnitude of (0.07, 0.40) pixel for the camera, and (0.07, 0.28) pixel for the projector. The low RMS error confirms the accuracy of the detection which benefits from the adapted projected pattern. Interestingly, the error is smaller for the projector calibration. This is explained by the fact that the ellipses used to calibrate the projector are extracted independently in each image, with high precision. Conversely, the printed markers used to calibrate the camera are assumed to lie on a regular grid, which might not be exactly true depending on the accuracy of the target. To assess the projective bias of ellipses' centers, the residual error was re-computed with the same calibration parameters but only considering the centers of the ellipses instead of projecting the conic. Depending on the orientation of the target with respect to the camera image, all points were affected by a systematic bias reaching up to 0.1 pixel. This bias is higher than the mean error and thus not appropriate for accurate measurements.

The radial distortion magnitude of the camera and projector are plotted in Fig.7 with respect to the radial distance from their principal points. The curves show a significant radial distortion component for both, the camera and projector. This confirms the importance to compensate lens distortion for the projector. We have also observed a shift of nearly 400 pixels for the projector principal point toward the top of the image. As noted in the previous section, this is due to the upward shift of the projector image with respect to the optical center of the lens assembly.

In order to assess the overall accuracy of the SLS, two objects were reconstructed and compared to precise models. We first evaluated the planarity of the reconstruction of a perfectly planar surface. The dimensions of the plane are 405x405mm and it is located at 1500mm in front of the SLS. To measure the surface, a grid of 20x20 photogrammetric targets was projected on the plane and triangulated.

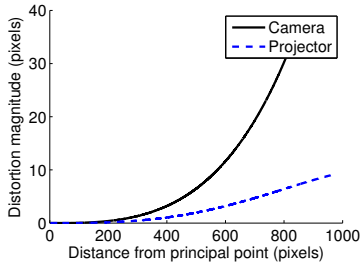

Figure 7. The radial distortion magnitude with respect to the principal point distance for the camera and projector.

They were localized in the camera image with the Forstner operator [1]. The projection of such targets ensures a purely geometric measure minimizing photometric factors.

The reconstructed surface is displayed in Fig.8(a). A plane was fitted to the 3D points and the mean and maximum value of the Euclidean distance between both is 0.10mm and 0.26mm respectively. An averaging filter was then applied to the surface to appreciate its curvature. The smoothed surface, displayed in Fig.8(b), exhibits a peak to peak curvature of approximately 0.2mm.

The second object is a resin-plaster head statue of $300^3 mm^3$ which is reconstructed at a distance of 1500mm. We performed two reconstructions and compared the surface with a precise model obtained from a laser range scanner. The SLS was calibrated before each reconstruction. The correspondence between the camera and projector coordinates was obtained by the projection of a combination of grey-code pattern followed by a phase-shift method [14]. The procedure returned 66149 points for the first scan and 77110 points for the second scan. The camera view and the alignment error of the recovered models, in mm, are displayed in Fig.9.

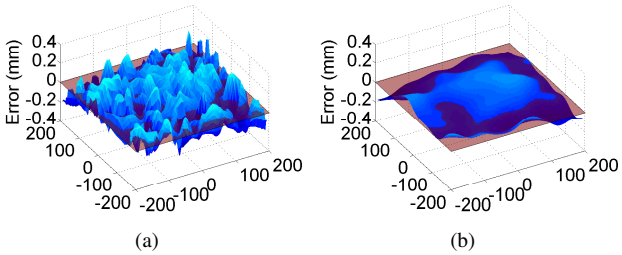

Figure 8. (a) The reconstructed surface of a plane along with the fitted plane shown in red. (b) The curvature of the surface obtained after noise filtering. (The axes are in mm)

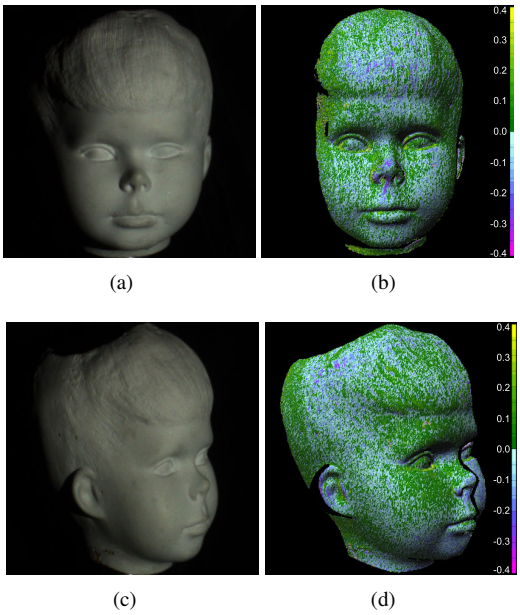

Figure 9. The 3D reconstructions of a real object from two viewpoints. The images on the left show the viewpoints of the object under the projection of a full white pattern whereas the right plots depict the alignment error of the reconstructed model (in mm).

The uniform distribution of the error suggests that there is no systematic bias in the reconstruction. The stronger noise near the nose in Fig.9(b) is caused by the acute angle of the projector light with the surface. The magnitude of the error is similar to that observed for the plane reconstruction in Fig.8 (both are displayed at the same scale). Furthermore, the two reconstructions exhibit a similar error which confirms the repeatability of the calibration method.

5. Conclusion

We have presented a rigorous and automatic method to accurately calibrate a SLS from circular control points. The method differs from previous works in that it is purely geometric and provides unbiased observation for the camera and projector calibration. In our setup, considering the projection of ellipse contours instead of centers allowed us to correct a bias reaching 0.1 pixel, which is more than the mean reprojection error. Instead of relying on a phase-shift method, or on the projection of stripes to find the correspondence between the camera and projector, we directly project calibration markers on the target. This is made possible by adapting the projected pattern to interleave between the printed markers. Furthermore, the projection maps ellipses to circles on the target, creating optimal conditions for the localization in the camera image. This resulted in a RMS calibration residual error of 0.07 pixel for both the projector and camera. Finally, we have demonstrated the accuracy and unbiasedness of the recovered parameters by comparing the reconstructed surface of a plane and of a head statue with precise models.

References

[1] W. Forstner and E. Gulch. A fast operator for detection and precise location of distinct points, corners and centres of circular features. In *Proc. Conf. on Fast Processing of Photogrammetric Data*, pages 281–305, 1987.

[2] J. Guhring, C. Brenner, J. Bohm, and D. Fritsch. Data processing and calibration of a cross-pattern stripe projector. *IAPRS*, 33(5):327–338, 2000.

[3] J. Heikkila. Geometric camera calibration using circular control points. *IEEE Trans. on Pattern Analysis and Machine Intelligence*, 22(10):1066–1077, 2000.

[4] T. Koninckx and L. V. Gool. Real-time range acquisition by adaptive structured light. *IEEE Trans. on Pattern Analysis and Machine Intelligence*, 28(3):432–445, March 2006.

[5] R. Legarda-Saenz, T. Bothe, and W. P. Juptner. Accurate procedure for the calibration of a structured light system. *Optical Engineering*, 43(2):464–471, 2004.

[6] Y. Ma, S. Soatto, J. Kosecka, and S. S. Sastry. *An Invitation to 3-D Vision*. Springer, 2003.

[7] J.-N. Ouellet and P. Hébert. A simple operator for very precise estimation of ellipses. In *Computer and Robot Vision*, pages 21–28, 2007.

[8] W. H. Press, S. A. Teukolsky, W. T. Vetterling, and B. P. Flannery. *Numerical Recipes in C: The Art of Scientific Computing*. Cambridge University Press, New York, NY, USA, 1992.

[9] S. Rusinkiewicz. Real-time acquisition and rendering of large 3d models. Ph.D. dissertation, Stanford University, 2001.

[10] F. Sadlo, T. Weyrich, R. Peikert, and M. Gross. A practical structured light acquisition system for point-based geometry and texture. *Eurographics: Symposium on Point-Based Graphics*, pages 89–145, 2005.

[11] R. J. Valkenburg and A. M. McIvor. Accurate 3d measurement using a structured light system. *Image and Vision Computing*, 16(2):99–110, 1998.

[12] G. Wang, Z. Hu, F. Wu, and H.-T. Tsui. Projector-camera based system for fast object modeling. IEEE International Workshop on Projector-Camera Systems, 2003.

[13] T. Weise, B. Leibe, and L. Van Gool. Fast 3d scanning with automatic motion compensation. *IEEE Conference on Computer Vision and Pattern Recognition*, pages 1–8, 2007.

[14] S. Zhang and P. Huang. High-resolution, real-time 3d shape acquisition. *Computer Vision and Pattern Recognition Workshop*, pages 28–28, 2004.

[15] Z. Zhang. A flexible new technique for camera calibration. *IEEE Trans. on Pattern Analysis and Machine Intelligence*, 22(11):1330–1334, Nov 2000.